Versatile hybrid optical waveguides in amorphous silicon carbide with enhanced functionality and performance

Khoshmehr, Mohammad Talebi; Dashtabi, Mahdi Mozdoor; Nikbakht, Hamed; Lopez Rodriguez, Bruno; Sharma, Naresh; Zadeh, Iman Esmaeil; van Someren, Bob; Akca, B. Imran

Citation (APA)
Khoshmehr, M. T., Dashtabi, M. M., Nikbakht, H., Lopez Rodriguez, B., Sharma, N., Zadeh, I. E., van Someren, B., & Akca, B. I. (2024). Versatile hybrid optical waveguides in amorphous silicon carbide with enhanced functionality and performance. *Applied Physics Letters*, *125*(11), Article 113505. https://doi.org/10.1063/5.0222085

Important note
To cite this publication, please use the final published version (if applicable).
Please check the document version above.

Versatile hybrid optical waveguides in amorphous silicon carbide with enhanced functionality and performance

Mohammad Talebi Khoshmehr ; Mahdi Mozdoor Dashtabi; Hamed Nikbakht ; Bruno Lopez Rodriguez ;
Naresh Sharma ; Iman Esmaeil Zadeh ; Bob van Someren; B. Imran Akca

Check for updates

View Online

Export Citation

Versatile hybrid optical waveguides in amorphous silicon carbide with enhanced functionality and performance

Mohammad Talebi Khoshmehr,[1] (iD) Mahdi Mozdoor Dashtabi,[1] Hamed Nikbakht,[1] (iD) Bruno Lopez Rodriguez,[2] (iD) Naresh Sharma,[2] (iD) Iman Esmaeil Zadeh,[2] (iD) Bob van Someren,[3] and B. Imran Akca[1,a] (iD)

AFFILIATIONS

[1]LaserLab, Department of Physics and Astronomy, VU University, De Boelelaan 1081, 1081 HV Amsterdam, The Netherlands
[2]Department of Imaging Physics (ImPhys), Faculty of Applied Sciences, Delft University of Technology, Delft, The Netherlands
[3]Elf Software, Mullerkade 667, 3024 EP Rotterdam, The Netherlands

[a]Author to whom correspondence should be addressed: b.i.avci@vu.nl

ABSTRACT

In most optical waveguides employed within photonic integrated circuits, light confinement is achieved by etching the high-index layer. However, these waveguides often lack versatility in optimizing optical properties, such as mode size, shape, dispersion, and polarization. Moreover, they frequently suffer from high coupling losses and their propagation losses are significantly influenced by the quality of the etching process, especially for materials with high mechanical rigidity. Here, we present a hybrid optical waveguide concept that effectively addresses these limitations by combining a strip of easily processible low-index material (SU8) with a high-index hard-to-etch guiding layer (amorphous silicon carbide, SiC). Our approach not only eliminates the need for SiC etching but also offers flexibility in waveguide design to accommodate advanced functionalities. One of the key advancements of this hybrid configuration is its ability to suppress the transverse magnetic mode by 62 dB at 1550 nm, effectively functioning as a transverse electric pass waveguide. This simplifies the measurements by eliminating the need for polarization controllers and polarizers. Furthermore, through tailored waveguides, we achieve 2.5 times higher coupling efficiency compared to untapered hybrid SiC waveguides. We also demonstrate that thermal baking of the polymer layer reduces the scattering losses from 1.57 to 1.3 dB/cm. In essence, our hybrid approach offers a versatile way of realizing low-loss SiC-based integrated optical components with advanced features, such as excellent polarization suppression, flexible mode shapes, and dispersion control, compared to etched counterparts.

Currently, the majority of photonic integrated circuits employ conventional etched optical waveguides, where light confinement is achieved by etching the high-index guiding layer.[1,2] However, the monolithic nature of etched waveguides restricts their versatility in optimizing optical properties, such as mode shape, size, dispersion, and polarization, limiting their ability to accommodate advanced functionalities. Furthermore, the high refractive index of the guiding layer often leads to a modal mismatch between fibers and waveguides, resulting in low coupling efficiencies and restricting practical applications. In addition, this approach imposes a significant challenge on fabricating dry-etched high-quality photonic components for materials that have a very stable chemical structure with strong mechanical rigidity (i.e., lithium niobate, barium titanate, silicon carbide).[3–5] Such devices usually have non-vertical sidewalls after dry etch, increasing the scattering losses and limiting the minimum gap between neighboring waveguides. Thus, it is of interest to explore hybrid waveguide configurations that combine a thin film of high-index material with an easy-to-etch photonic material (e.g., polymers, amorphous silicon, and silicon nitride) in a loaded strip structure[6] to provide a more versatile platform while avoiding dry etching of the guiding layer. Among these possible materials, UV-curable transparent polymers offer distinct advantages. They do not need advanced etching technology to form optical waveguides[7–11] and a simple chemical etching suffices to pattern structures on the wafer. However, commercially available polymers often have a low refractive index ($n = 1.5$–1.6), which increases the optical mode size and hence the device footprint, making it

23 September 2024 09:31:53

unsuitable for high-density photonic circuits. Exploiting the bound states in the continuum (BIC) concept,[12] hybrid waveguides using a low-index polymer loading layer were demonstrated.[13] However, BIC's nature limits the lowest loss to specific bending radii, restricting its applicability.

Here, we present a versatile, etch-free hybrid optical waveguide structure that exhibits excellent polarization suppression (>62 dB) and high coupling efficiency (2.5 times higher) compared to its etched counterparts. The waveguide integrates an easily processable low-index polymer, i.e., SU8, with a thin film of high-quality amorphous silicon carbide (a-SiC)[14] using our recent waveguide concept tailored for low-index contrast systems[9,24] [Figs. 1(a) and 1(b)]. Recently, SiC has gained significant attention[15–17] for integrated photonic device applications due to its exceptional optical properties.[18–21] While a-SiC can be etched using SF_6, it is more challenging than etching silicon or silicon dioxide due to its strong covalent bonds. Current SiC waveguides exhibit propagation losses ranging from 0.38 to 3 dB/cm.[4,14,22,23] In this study, we achieved a propagation loss of 1.3 dB/cm (dominated by the polymer absorption) through our etch-free approach and improved a-SiC deposition method. We believe our hybrid waveguide concept and its enhanced functionalities offer valuable insights for diverse photonic components across various applications.

Realizing compact PICs in low-index contrast material platforms can be challenging. We address this problem by employing a suitably customized hybrid waveguide,[9,24] formed by combining a high-index guiding layer of refractive index n_g with a lower-index loading layer of refractive index n_p [Fig. 1(a)]. The thicknesses of the guiding layer, t_g, and of the loading layer, t_p, are chosen in such a way that two weakly guiding regions with near-cutoff optical modes are created, which are subsequently coupled to form an optical waveguide with strong mode confinement. This design approach ensures a low-loss optical mode with reduced contributions from material and radiation losses to the overall modal attenuation. In our waveguide simulations, we employed the beam propagation method (BPM) using RSoft Inc. software. The refractive indices for the thermal oxide, polymer layer, and a-SiC layer at $\lambda = 1550$ nm were set to 1.45, 1.58, and 2.57, respectively. The waveguide width was chosen to be $w = 1.5\,\mu m$ to ensure guidance of only the fundamental mode. All calculations presented in Figs. 1(c)–1(e) were based on this chosen width.

We formed optical waveguides using ICPCVD-deposited a-SiC as the guiding layer and SU8 (6000, MicroResist Technology GmbH) as the loading layer. The central wavelength of 1550 nm is used in calculations and simulations. For the guiding layer, the effective refractive index of the fundamental mode (G_{neff}) is calculated for the t_g values ranging between 40 and 140 nm [Fig. 1(c)]. As can be seen from this
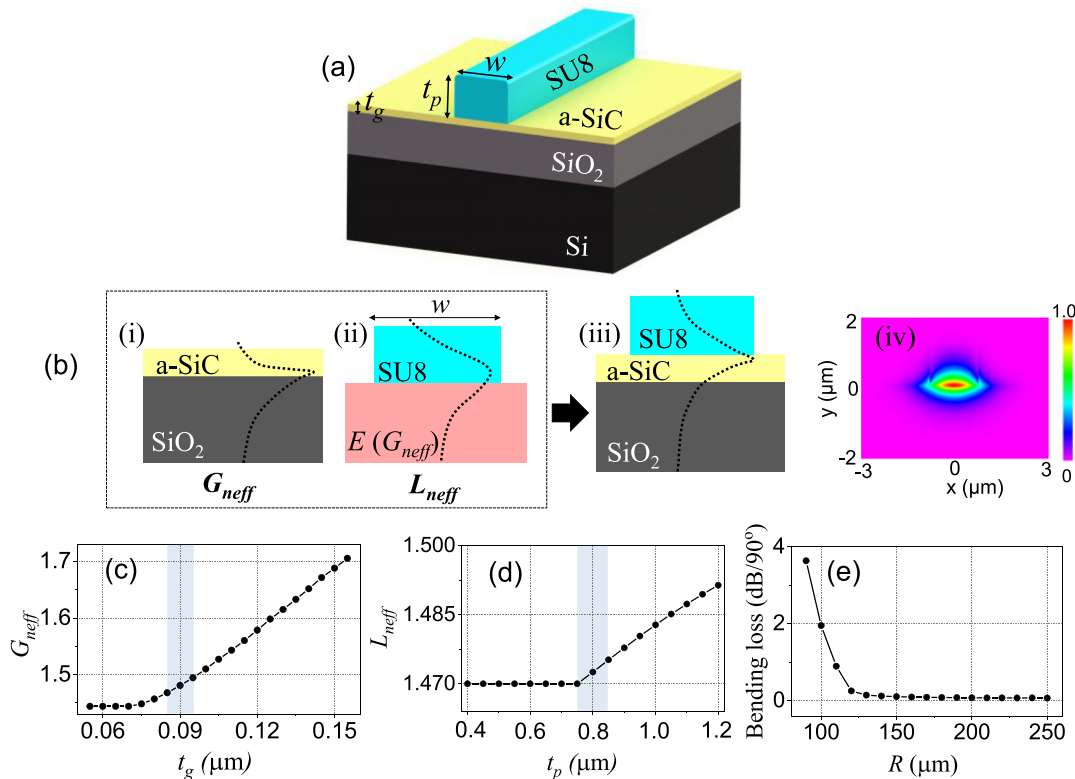
FIG. 1. (a) Schematic of the hybrid a-SiC optical waveguide. (b) The vertical mode profiles in the (i) guiding (a-SiC) and (ii) loading (SU8) layers. The right image (iii) shows the confined mode formed by combining these weakly confined vertical optical modes and (iv) is the 2D mode profile of the waveguide for optimum thickness values of the SU8 and a-SiC layers obtained from (c) and (d). The simulated effective refractive indices of the hybrid waveguide for different thicknesses of (c) a-SiC (t_g) and (d) SU8 (t_p). The optimum values of the a-SiC and the SU8 layers are shown with light-blue rectangles. (e) Bending loss vs bending radius for the hybrid waveguide structure given in (iii) with $t_g = 90$ nm and $t_p = 800$ nm.

figure, the light mostly travels in the bottom SiO$_2$ cladding when $t_g \leq 90$ nm. So, the thickness that can weakly confine the light in this layer (i.e., close to cutoff) is extracted as 90 ± 5 nm. We applied the same approach to the loading layer and calculated the effective refractive index (L_{neff}) of the fundamental mode as given in Fig. 1(d). The mode mostly travels in the bottom effective layer when $t_p \leq 800$ nm. Therefore, the cutoff value of t_p is extracted as 800 ± 50 nm, which corresponds to weak vertical confinement as well. The 2D mode profile of the waveguide for the optimal values of a-SiC and SU8 layers are shown in Fig. 1(b-iv). The margins represent the range within which the waveguide operates with minimal loss while maintaining a compact size. We scanned the thickness values for each layer and calculated the corresponding loss and bending radius for each combination. Based on these results, we defined the operational margins for each layer.

The bending loss of the hybrid waveguide was calculated for the bending radius range of $R = 80$–$250\,\mu$m [Fig. 1(e)]. Using the simulated bend method of RSoft Inc. software, the minimum bending radius that results in a bending loss value of 0.005 dB/90° was extracted as $R = 150\,\mu$m. To calculate the bending loss, the imaginary part (n_i) of the effective refractive index of optical modes in the bent waveguide was used in the loss formula $L\left(dB/cm\right) = 4.343 \cdot \gamma\left(cm^{-1}\right)$, where $\gamma = \frac{4\pi}{\lambda} n_i$ is the loss coefficient. In the simulations, scattering was not included. We measured the absorption loss of the SU8 layer as ~ 3 dB/cm using a custom interferometry-based method, extracting the extinction coefficient as 8.3×10^{-6}. In this method, we apply a thick SU8 layer ($>150\,\mu$m) to a transparent substrate, expose and bake it, then measure the 1550 nm SLED light transmission and calculate absorption loss, accounting for surface reflections and layer thickness. For the a-SiC layer, we estimated a maximum extinction coefficient of approximately 2×10^{-6} using the minimum loss value provided in Ref. 14 (i.e., 0.78 dB/cm). The loss value, measured on etched ICPCVD-deposited a-SiC waveguides, includes both material absorption and scattering. Thus, the estimated extinction coefficient for the a-SiC layer represents the maximum value. Using this coefficient, the material absorption loss for the hybrid waveguide was simulated at 1.25 dB/cm.

For the fabrication of waveguides, a thin layer of a-SiC was deposited on a commercial 8-μm-thick thermally oxidized silicon wafer using the optimized ICPCVD method from Ref. 14. The vertical mode profile of the fabricated device is given in Fig. 1(b-iii). An air cladding was used to reduce the optical loss caused by SU8 absorption. For high-density integration, a low-index polymer with a refractive index of ~ 1.15 (e.g., Inkron resins) can be used. The devices were fabricated using e-beam writing; however, no conductive polymers were used to define the structures in contrast to common practice. The SU8 layer was directly exposed, which reduced the fabrication steps and eliminated the contamination of residuals of conductive polymer. To achieve this, we developed an unconventional e-beam writing process by reducing the exposure dose (3 uC/cm^2) and increasing the writing speed (200 mm/s) as well as the resolution (10 nm). This step was followed by developing exposed samples with 1-methoxy-2-propanol acetate. The measured width of the fabricated waveguides was $1.50 \pm 0.05\,\mu$m. The fabricated devices were cleaved but facets were not polished.

The optical loss value of the hybrid a-SiC waveguides was extracted from the racetrack resonator measurement results. We used our custom measurement method, the so-called sweeping optical

frequency mixing method (SOHO),[25,26] to measure the full width at half maximum (FWHM) of the fabricated resonators. It is comprised of a tunable laser (EMCORE TTX1995 micro-ITLA, called sample laser), a fixed wavelength laser (Thorlabs, WDM8-C-23A-20 nm, called reference laser), a photodiode (Thorlabs, DET08CFC/M), and an electric spectrum analyzer (ESA, Signal Hound, BB60D) as shown in Fig. 2. This system operates in real-time and provides very high resolution (19.1 fm) and 30-dB higher sensitivity than a high-resolution tunable laser system. The added value of SOHO becomes more apparent when applied to cavities with ultra-high-quality factors. A detailed description of this measurement method is given in Ref. 26.

To extract the optical loss (α) of the hybrid waveguides, we utilized racetrack resonators and calculated α using the following formula:[27]

$$\alpha(dB/cm) = 4.34 \times \frac{\lambda_0}{Q_{\mathrm{int}} \times FSR \times R}, \qquad (1)$$

where λ_0 is the resonant wavelength, FSR is the free spectral range, and R is the radius of the racetrack resonator. Q_{int} is the intrinsic quality factor, calculated using the transmitted optical power at the resonant wavelength and the FWHM of the resonant peak as explained in Ref. 28. The resonator is not a circular ring; however, its effective radius can be calculated using the following formula:[27]

$$R_{eff} = \frac{C}{2\pi}, \qquad (2)$$

where C is the circumference of the racetrack resonator. We designed several racetrack resonators with varying coupling lengths, all with $R = 150\,\mu$m. The best coupling length that provides close to critical coupling was found to be $L_c = 50\,\mu$m. The corresponding effective radius was calculated as $R_{eff} = 166\,\mu$m. The FWHM value of the resonance peak at $\lambda = 1550$ nm was measured as 11 pm, which corresponds to $Q_{int} = 2.24 \times 10^5$ [Fig. 3(a), bottom]. Note that the bandwidth of the SOHO system is limited to 12 GHz by the tunable laser range, therefore only a few resonances can be measured at any given time. We post-baked the fabricated devices at 170 °C for an hour using a hot plate and the FWHM of the same racetrack resonator
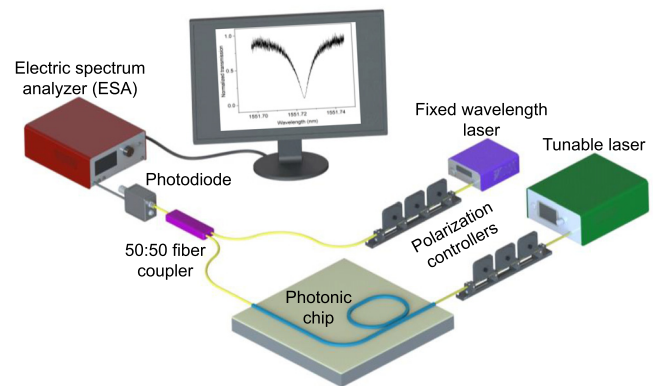

FIG. 2. Measurement setup. Light from a tunable laser is coupled to the photonic chip via a polarization controller. The output of the photonic chip is mixed with light from a fixed-wavelength laser in a 50:50 fiber coupler and sent to an electric spectrum analyzer through a photodiode.
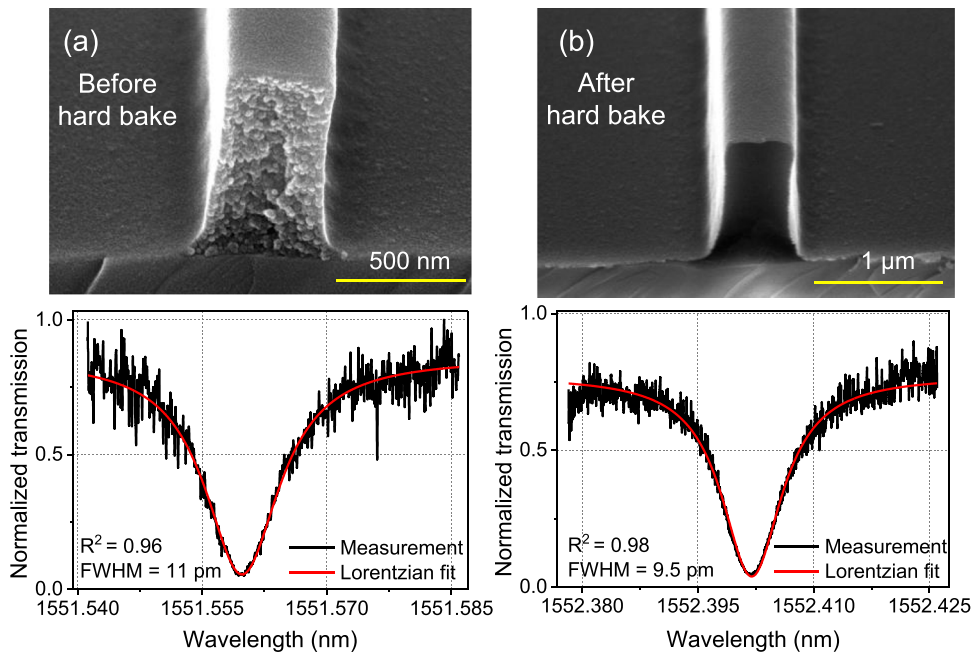
FIG. 3. The SEM images of the waveguide cross sections of the racetrack resonators (a) before and (b) after the hard bake step. The transmission measurements of the racetrack resonators are shown below, normalized to each data set's maximum for clarity. The red line represents the Lorentzian fit to the experimental data.

decreased to 9.5 pm, corresponding to $Q_{int} = 2.7 \times 10^5$ [Fig. 3(b), bottom]. Without post-baking, the optical loss increases by 21%.

The scanning electron microscope (SEM) images of the waveguide cross section before and after the thermal hard bake step are provided in Figs. 3(a) and 3(b), respectively. As can be seen from Fig. 3(a), the SU8 layer exhibits a granular texture, characterized by particle sizes of approximately 30–50 nm. These particles scatter the light, consequently increasing the optical loss. As shown in Fig. 3(b), annealing reduces the size of scatters in the SU8 layer significantly and smoothens the layer. We also observed a small red shift of 0.84 nm, following the thermal hard bake step, which can be due to the slight refractive index change of the SU8 layer. Inserting $Q_{int} = 2.7 \times 10^5$ and the effective radius of the racetrack resonator to Eq. (1), the optical loss was calculated to be $\alpha = 1.3$ dB/cm, which is mainly dominated by material absorption of the SU8 layer.

Given its hybrid nature, our waveguide structure inherently does not support TM-polarized light but efficiently transmits TE-polarized light with minimal loss, rendering it an ideal TE-pass waveguide[29–33] with an exceptionally high polarization extinction ratio. Moreover, wider multimode waveguides support TM modes [Fig. 4(c)], allowing TM-polarized light to be handled on the same chip using polarization rotators made from these waveguides. We used the experimental setup given in Fig. 4(a), which is comprised of a distributed feedback laser centered at 1550 nm (EMCORE TTX1995 micro-ITLA), an in-line fiber polarizer (Thorlabs, ILP1550SM-FC), two polarization controllers (PC1, PC2), and an OSA. First, we aligned PC1 to maximize light power following the polarizer. Then, we aligned PC2 to selectively couple TE- or TM-polarized light into the SU-8 loaded SiC optical waveguide, and finally, we measured the output power with the OSA. Optical waveguides with three different lengths, i.e., 5, 7.2, and 8.7 mm, were measured, and a polarization extinction ratio of 62 dB was achieved for a waveguide length of 8.7 mm [Fig. 4(b)]. The curve flattens around 8.7 mm because the output signal weakens beyond this

length, making detection difficult and polarization control challenging. Thus, the 62 dB measurement reflects setup constraints rather than device limitations.

We simulated the coupling loss of the waveguide for TE- and TM-polarized light for different waveguide widths as shown in Fig. 4(c). For each width, the effective refractive index of the mode at a wavelength of 1550 nm was calculated using the Lumerical mode solver. This calculation was performed for both TE and TM polarizations, with a Gaussian input field. The imaginary part of the refractive index was then used to determine the corresponding loss values for each width. As can be seen, the loss is significantly larger for the TM mode due to its weak confinement and there is an inverse relation between the loss of the TE and TM modes for increasing waveguide widths.

High coupling loss between waveguides and optical fibers is a serious problem for high-index materials such as Si and SiC. The hybrid nature of our waveguide platform partially solves this problem due to the inherent larger mode size. Inverse tapers increase the mode size [Fig. 5(b)] and make it possible to match it with the optical mode of the fiber in contrast to non-tapered regular waveguides [Fig. 5(a)]. We simulated the coupling efficiency of the hybrid waveguide for different inverse taper widths (i.e., the width of the SU8 layer) using the finite difference time domain method (FDTD, Lumerical Inc.). To do so, a fiber mode (SMF-28) of 10.4 ± 0.8 μm size was fed into the waveguide and the transmitted light was recorded for different taper widths at 1550 nm. As can be seen in Fig. 5(c), the coupling efficiency becomes 18.6% for a taper width of 200 nm and it reduces to 11% when no taper is applied (width = 1.5 μm). However, for taper widths <400 nm, we observed that the SU8 layer tilts over (i.e., bends and collapses to the side) as shown in the SEM image [Fig. 5(f)]. Therefore, we used a taper width of 400 nm, which was fabricated without any problems [Fig. 5(e)]. The coupling efficiency for this taper width was estimated to be 17.5% from the FDTD simulations. When these values are used to compare the transmitted optical power in tapered and
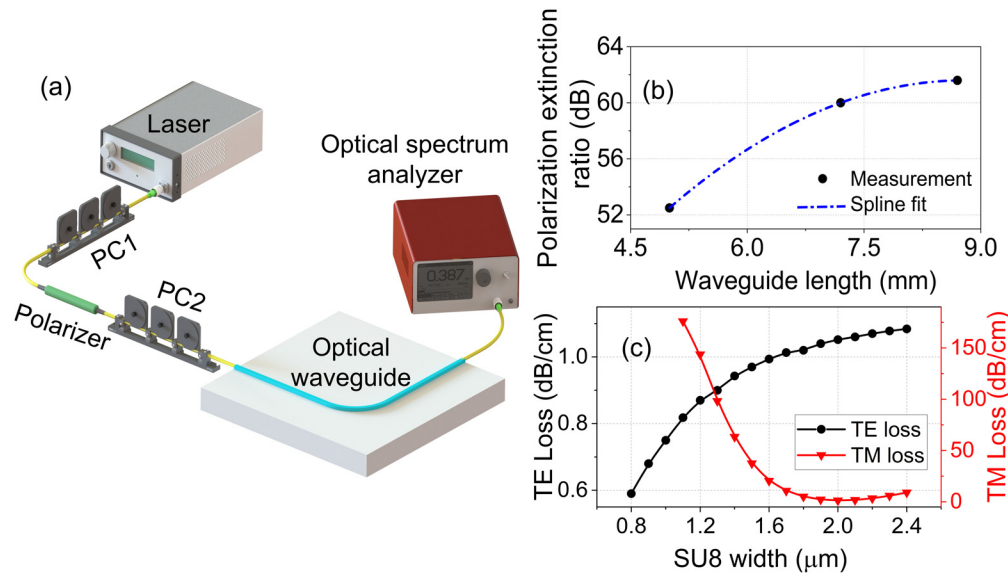
23 September 2024 09:31:53

FIG. 4. (a) Polarization measurement setup. PC1 and PC2 are polarization controllers. (b) Measured TM suppression ratio for three waveguide lengths: 5, 7.2, and 8.7 mm. The blue dashed line is the spline fit. (c) Simulation results of the loss for the TE (black line) and TM modes (red line) for different waveguide widths.

untapered waveguides, we expect 2.53 times $[(17.5)^2/(11)^2 = 2.53$, square accounts for input and output coupling] higher optical power in the tapered waveguides. Our transmission measurements, conducted on both regular (untapered) and tapered waveguides [Fig. 5(d)], confirm the simulated results, showing approximately 2.5 times higher optical power for the tapered waveguide compared to the regular one at 1550 nm. The difference in period of the Fabry–Pérot

(FP) oscillations between tapered and regular waveguides arises from variations in the effective refractive index (lower for the tapered waveguides) and small differences in waveguide physical lengths.

In conclusion, we demonstrated the added functionalities (i.e., excellent polarization suppression, higher coupling efficiency, and reduced losses through thermal baking) and simplified fabrication procedure offered by our hybrid etch-free waveguide concept, particularly
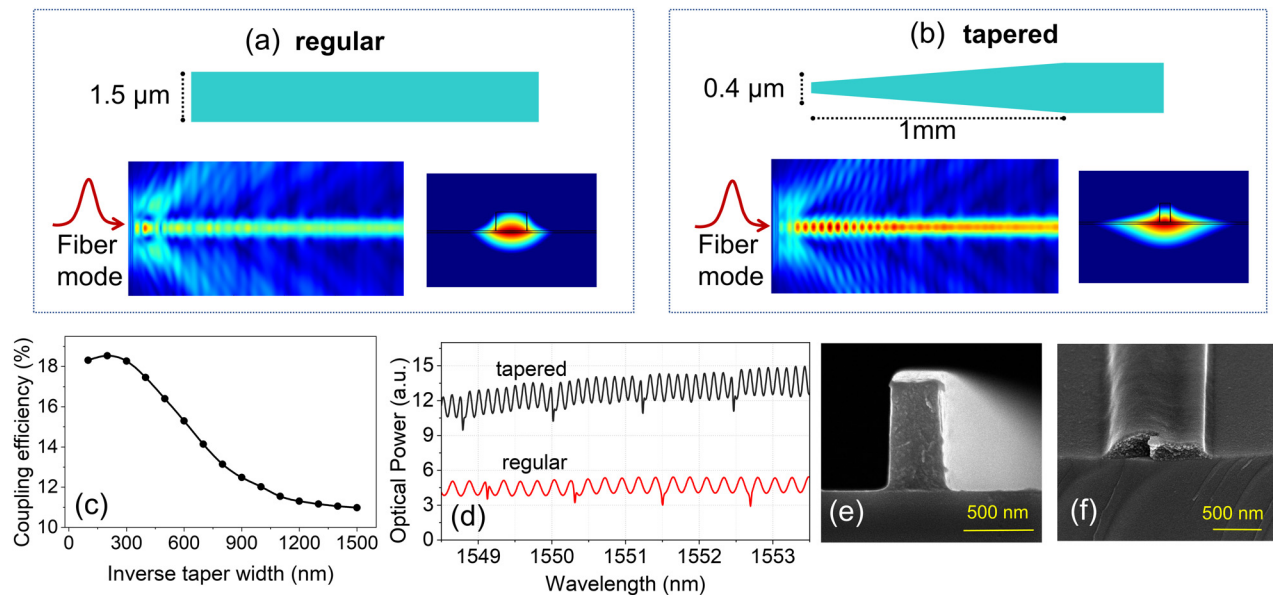
FIG. 5. Top view of the waveguides with a (a) regular (untapered) and (b) tapered facet. The field propagation and the mode profile for the regular and tapered waveguides are given in the bottom row of each figure. (c) Simulation results of the coupling efficiency for different inverse taper widths. (d) Transmission measurement results of the regular and tapered facet waveguides representing improvement in the coupling efficiency. SEM images of the tapered facet waveguide with a width of (e) 400 and (f) 300 nm. As seen, the polymer layer tilted over for the 300 nm taper width.

benefiting materials that are difficult to etch. The etch-free nature of this process provides significant advantages across various applications. The reduced scattering loss can provide superior performance in on-chip fluorescent imaging,[34] flow cytometry,[35] and quantum photonics.[36] For devices utilizing piezoelectric materials (i.e., lithium niobate), the etch-free process ensures smooth propagation of surface acoustic waves, which is crucial for developing high-performance modulators and switches used in optical signal processing.[37] To improve coupling efficiency, lensed fibers with custom mode sizes matched to the hybrid waveguides can be used (HighRI Optics). The main source of optical loss in current waveguides is SU8 material absorption, which can be reduced with transparent polymers or hybrid chalcogenides. Hybrid chalcogenides also provide a more rigid and reliable alternative to polymer loading layers, improving edge coupling. We believe our etch-free hybrid waveguide approach, with its enhanced characteristics and versatility, can serve as an agile platform for advancing emerging integrated photonics applications.

See the supplementary material for details on the removal of Fabry–Pérot oscillations using angled facet waveguides, Mach–Zehnder interferometer design and measurements, and comparison between cut-back and race-track resonator-based loss measurements.

AUTHOR DECLARATIONS
Conflict of Interest

The authors have no conflicts to disclose.

Author Contributions

Mohammad Talebi Khoshmehr: Conceptualization (supporting); Data curation (lead); Formal analysis (equal); Investigation (lead); Methodology (lead); Software (equal); Validation (equal); Visualization (equal). **Mahdi Mozdoor Dashtabi:** Data curation (equal); Formal analysis (equal); Methodology (equal). **Hamed Nikbakht:** Conceptualization (equal); Methodology (equal); Supervision (equal). **Bruno Lopez-Rodriguez:** Data curation (equal); Resources (equal). **Naresh Sharma:** Resources (equal). **Iman Esmaeil Zadeh:** Investigation (supporting); Resources (equal). **Bob van Someren:** Conceptualization (equal); Methodology (equal). **B. Imran Akca:** Conceptualization (equal); Formal analysis (equal); Funding acquisition (equal); Methodology (equal); Project administration (equal); Supervision (equal); Writing – original draft (equal); Writing – review & editing (equal).

DATA AVAILABILITY

The data that support the findings of this study are available from the corresponding author upon reasonable request.

REFERENCES

[1]C. G. H. Roeloffzen, M. Hoekman, E. J. Klein *et al.*, "Low-loss Si₃N₄ triPleX optical waveguides: Technology and applications overview," IEEE J. Sel. Top. Quantum Electron. **24**(4), 1–21 (2018).

[2]A. Melloni, R. Costa, G. Cusmai, and F. Morichetti, "The role of index contrast in dielectric optical waveguides," Int. J. Mater. Product Technol. **34**(4), 421–437 (2009).

[3]Z. Ren, P. J. Heard, J. M. Marshall, P. A. Thomas, and S. Yu, "Etching characteristics of LiNbO₃ in reactive ion etching and inductively coupled plasma," J. Appl. Phys. **103**, 034109 (2008).

[4]P. Xing, D. Ma, K. J. A. Ooi, J. W. Choi, A. M. Agarwal, and D. Tan, "CMOS-compatible PECVD silicon carbide platform for linear and nonlinear optics," ACS Photonics **6**, 1162–1167 (2019).

[5]A. Karvounis, F. Timpu, V. V. Vogler-Neuling, R. Savo, and R. Grange, "BaTiO₃: Barium titanate nanostructures and thin films for photonics," Adv. Opt. Mater. **8**, 2070094 (2020).

[6]V. Ramasamy, "Strip-loaded film waveguide," Bell Syst. Tech. J. **53**, 697 (1974).

[7]M. A. A. Neil, J. P. Sharpe, E. G. S. Paige, M. J. Cherrill, S. E. Broomfield, and S. J. Sheard, "Strip loaded polymeric optical waveguides with low loss," in *Integrated Photonics Research, Technical Digest Series* (Optica Publishing Group, 1991), Paper No. ThA8.

[8]L. Ahmadi, V. Kontturi, J. Laukkanen, M. Kuittinen, J. Saarinen, S. Honkanen, and M. Roussey, "Polymer striploaded waveguides on ALD-TiO₂ films," Proc. SPIE **9759**, 97590D (2016).

[9]H. Nikbakht, B. van Someren, M. Hammer, and B. I. Akca, "Weak optical modes for high-density and low-loss photonic circuits," APL Photonics **8**, 056107 (2023).

[10]J. Yang, "Neodymium-doped waveguide amplifiers and lasers for integrated optical applications," Ph.D. thesis (University of Twente, 2010).

[11]J. Xiong, E.-L. Hsiang, Z. He, T. Zhan, and S.-T. Wu, "Augmented reality and virtual reality displays: Emerging technologies and future perspectives," Light **10**, 216 (2021).

[12]J. V. Neumann and E. Wigner, "On some peculiar discrete eigenvalues," Physica Z **30**, 465 (1929).

[13]Y. Yu, Z. Yu, L. Wang, and X. Sun, "Ultralow-loss lithium niobate integrated photonics at near-visible wavelengths," Adv. Opt. Mater. **9**, 2100060 (2021).

[14]B. Lopez-Rodriguez, R. van der Kolk, S. Aggarwal, N. Sharma, Z. Li, D. van der Plaats, T. Scholte, J. Chang, S. Gröblacher, S. F. Pereira, H. Bhaskaran, and I. E. Zadeh, "High-quality amorphous silicon carbide for hybrid photonic integration deposited at a low temperature," ACS Photonics **10**, 3448 (2023).

[15]Y. Zheng, M. Pu, A. Yi, X. Ou, and H. Ou, "4H-SiC microring resonators for nonlinear integrated photonics," Opt. Lett. **44**, 5784 (2019).

[16]T. Fan, X. Wu, S. R. M. Vangapandu, A. H. Hosseinnia, A. A. Eftekhar, and A. Adibi, "Racetrack microresonator based electro-optic phase shifters on a 3C silicon-carbide-on-insulator platform," Opt. Lett. **46**, 2135 (2021).

[17]C. Wang, Z. Fang, A. Yi, B. Yang, Z. Wang, L. Zhou, C. Shen, Y. Zhu, Y. Zhou, R. Bao, Z. Li, Y. Chen, K. Huang, J. Zhang, Y. Cheng, and X. Ou, "High-Q microresonators on 4H-silicon-carbide-on-insulator platform for nonlinear photonics," Light **10**, 139 (2021).

[18]S. Wang, M. Zhan, G. Wang, H. Xuan, W. Zhang, C. Liu, C. Xu, Y. Liu, Z. Wei, and X. Chen, "4H-SiC: A new nonlinear material for midinfrared lasers," Laser Photonics Rev. **7**, 831 (2013).

[19]I. J. Wu and G. Y. Guo, "Second-harmonic generation and linear electro-optical coefficients of SiC polytypes and nanotubes," Phys. Rev. B **78**, 035447 (2008).

[20]R. Adair, L. L. Chase, and S. A. Payne, "Nonlinear refractive index of optical crystals," Phys. Rev. B **39**, 3337 (1989).

[21]P. T. B. Shaffer, "Refractive index, dispersion, and birefringence of silicon carbide polytypes," Appl. Opt. **10**, 1034–1036 (1971).

[22]T. Fan, H. Moradinejad, X. Wu, A. A. Eftekhar, and A. Adibi, "High-Q integrated photonic microresonators on 3C-SiC-on-insulator (SiCOI) platform," Opt. Express **26**, 25814–25826 (2018).

[23]M. A. Guidry, D. M. Lukin, K. Y. Yang, R. Trivedi, and J. Vuckovic, "Quantum optics of soliton microcombs," Nat. Photonics **16**, 52–58 (2021).

[24]B. I. Akca and B. van Someren Waveguide, UK Patent No. GB2009731.7 (16 June 2021).

[25]M. Dashtabi and B. I. Akca, "System and method for interrogating a photonic circuit," European Patent No. 23199844.4 (26 September 2023).

[26]M. M. Dashtabi, M. T. Khoshmehr, H. Nikbakht, B. L. Rodriguez, N. Sharma, I. E. Zadeh, and B. I. Akca, "Real-time measurements of photonic microchips with femtometer-scale spectral precision and ultra-high sensitivity," Laser Photonics Rev. **18**, 2301396 (2024).

[27]A. Griffith, J. Cardenas, C. B. Poitras, and M. Lipson, "High quality factor and high confinement silicon resonators using etchless process," Opt. Express **20**, 21341 (2012).

[28]P. An, V. Kovalyuk, A. Golikov, E. Zubkova, S. Ferrari, A. Korneev, W. Pernice, and G. Goltsman, "Experimental optimisation of O-ring resonator Q-factor for on-chip spontaneous four wave mixing," J. Phys.: Conf. Ser. **1124**, 051047 (2018).

[29]L. He, M. Zhang, A. Shams-Ansari, R. Zhu, C. Wang, and L. Marko, "Low-loss fiber-to-chip interface for lithium niobate photonic integrated circuits," Opt. Lett. **44**, 2314–2317 (2019).

[30]P. Chamorro-Posada, "Ultracompact integrated polarizers using bent asymmetric coupled waveguides," Opt. Lett. **44**, 2040–2043 (2019).

[31]H. Zafar, Y. Zhai, J. E. Villegas, F. Ravaux, K. L. Kennedy, M. F. Pereira, M. Rasras, A. Shamim, and D. H. Anjum, "Compact broadband (O, E, S, C, L & U bands) silicon TE-pass polarizer based on ridge waveguide adiabatic S-bends," Opt. Express **30**, 10087–10095 (2022).

[32]J. F. Bauters, M. J. R. Heck, D. Dai, J. S. Barton, D. J. Blumenthal, and J. E. Bowers, "Ultralow-loss planar Si_3N_4 waveguide polarizers," IEEE Photonics J. **5**, 6600207–6600207 (2013).

[33]H. Xu, D. Dai, and Y. Shi, "Ultra-broadband and ultra-compact on-chip silicon polarization beam splitter by using hetero-anisotropic metamaterials," Laser Photonics Rev. **13**, 1800349 (2019).

[34]Ø. I. Helle, D. A. Coucheron, J. Ce Tinguely, C. I. Øie, and B. S. Ahluwalia, "Nanoscopy on-a-chip: Super-resolution imaging on the millimeter scale," Opt. Express **27**, 6700–6710 (2019).

[35]S. Jooken, K. Zinoviev, G. Yurtsever *et al.*, "On-chip flow cytometer using integrated photonics for the detection of human leukocytes," Sci. Rep. **14**, 10921 (2024).

[36]N. Chauhan, J. Wang, D. Bose, K. Liu, R. L. Compton, C. Fertig, C. W. Hoyt, and D. J. Blumenthal, "Ultra-low loss visible light waveguides for integrated atomic, molecular, and quantum photonics," Opt. Express **30**, 6960–6969 (2022).

[37]L. Cai, A. Mahmoud, M. Khan, M. Mahmoud, T. Mukherjee, J. Bain, and G. Piazza, "Acousto-optical modulation of thin film lithium niobate waveguide devices," Photonics Res. **7**, 1003–1013 (2019).